Pergamon

Electrochimica Acta, Vol. 39, No. 17, pp. 2619–2628, 1994
Copyright © 1994 Elsevier Science Ltd.
Printed in Great Britain. All rights reserved
0013–4686/94 \$7.00 + 0.00

0013–4686(94)00204–5

KINETICS OF COPPER PASSIVATION AND PITTING CORROSION IN Na_2SO_4 CONTAINING DILUTE NaOH AQUEOUS SOLUTION

R. M. Souto, S. González, R. C. Salvarezza* and A. J. Arvia*

Departamento de Química Física, Universidad de La Laguna, Tenerife, Spain
*INIFTA, Universidad Nacional de La Plata, La Plata, Argentina

(*Received* 5 *January* 1994; *in revised form* 21 *April* 1994)

Abstract—The electrochemical behaviour of Cu in alkaline solutions containing Na_2SO_4 was studied using potentiodynamic and potentiostatic techniques complemented by scanning electron microscopy. The presence of Na_2SO_4 enhances Cu electrodissolution through the passive layer and decreases the breakdown potential. There is a critical OH^-/sulphate concentration ratio for the onset of localized corrosion. The competitive interaction between OH^- and sulphate ions at the passive layer can explain the experimental data. Pit initiation fits the point defect model for passivity breakdown. Pit growth involves a number of current contributions which can be distinguished through the analysis of current transients at constant potential by using nucleation and growth models.

Key words: copper, copper passivation, pitting corrosion, sulphate solutions, nucleation, growth processes.

1. INTRODUCTION

The electrochemistry of copper in alkaline solutions has been investigated in relation to the protective characteristics of passive films and the electrochemical production of Cu oxide layers[1–13]. The characteristics of electrochemically formed Cu oxides are closely related to the structure and morphology of these films, which in turn depend on the kinetics of oxide film formation.

The formation of anodic Cu oxide layers takes place over a relatively broad potential range within the stability potential range of water. The composition and water content of these Cu oxide layers depend considerably on the applied potential, and under certain conditions, also on the electrolysis time[1, 2, 4, 5, 9, 10]. In moderate alkaline solutions, Cu passivity has been explained by the formation of a duplex structured oxide layer[6, 7], consisting in general terms of an inner Cu_2O and an outer CuO layer. The formation of Cu oxide layers is accompanied by the appearance of Cu(I) and Cu(II) soluble species[8, 9] and, depending on the nature of anions present in the solution, insoluble Cu salts can also be formed, usually precipitated on the Cu oxide layer.

Passivity breakdown and copper pitting initiation take place beyond the critical breakdown potential (E_b) of the passive layer[3, 7]. The value of E_b strongly depends on the solution composition, and inferred from the passivity breakdown of copper in aqueous solutions containing Cl^-[7, 13], Br^-[14], ClO_4^-[15], SCN^-[16, 17], S^{2-}[18], CO_3^{2-} and HCO_3^- ions[11]. Otherwise, insoluble salt deposits are sometimes capable of blocking pit growth on Cu specimens at potentials more positive than E_b[11]. Copper pitting corrosion induced by sulphate ions has been reported by several authors[19–21]. In neutral Na_2SO_4 containing aqueous solutions, sulphate ions increase Cu oxide film formation in the passivation potential range, as well as the anodic Cu electrodissolution in the transpassive potential region[21]. Passivity breakdown of Cu involves a pit nucleation stage followed by pit growth[21]. Nevertheless, the knowledge of the kinetics and mechanism of copper corrosion, passivation and passivity breakdown in sulphate-ion-containing aqueous alkaline solutions still requires further investigation to determine the likely reaction models prevailing at each stage, and also to establish the validity of these models.

The main purpose of this work is to investigate the mechanism of Cu electro-oxidation through Cu oxide coatings, and Cu pitting in Na_2SO_4-containing dilute NaOH solutions. As each one of these processes becomes relevant within defined potential ranges, it is possible to explore their kinetics through the analysis of anodic current transients obtained at constant potentials. As the electrochemical behaviour of the system resembles to some extent that already decribed for Cu in alkaline solutions containing aggressive ions, the model previously described for the passivity and pitting corrosion of Cu can be used[7, 14].

This paper shows that the electrochemical behaviour of Cu in Na_2SO_4-containing dilute aqueous NaOH involves anodic oxide layer growth, anodic Cu electrodissolution through the passive layer, and Cu pitting. Potentiostatic and potentiodynamic data

indicate that the influence of Na_2SO_4 appears already at the initial stages of Cu oxide formation through a competitive adsorption between OH^- and sulphate ions at the Cu surface. Passivity breakdown can be explained as a vacancy diffusion from the Cu/oxide interface to the oxide/solution enhanced by anion adsorption. A model based on the heterogeneous nucleation and growth theory is advanced to account for the kinetics of pit growth.

2. EXPERIMENTAL

A conventional three-electrode electrochemical cell was used. Working electrodes (specimens) consisted of flat Cu discs (0.3 cm dia.) resulting from the axial cutting of electrolytic Cu rods. The working electrode surface of each specimen was first mechanically polished by employing a sequence of 30–5 μm grit (silicon carbide) emery papers, then degreased, rinsed with distilled water, and finally dried in air. To eliminate residual mechanical stresses, one set of those specimens was annealed at 500°C for 2 h under a few mm Ar gas pressure, following the procedure described elsewhere[12]. Also, thermally treated Cu specimens were electropolished in 85% H_3PO_4 at $0.3\,A\,cm^{-2}$ for 5–10 min at room temperature. Finally, they were thoroughly rinsed with distilled water and dried in air.

Each Cu specimen was axially mounted at the end of a vertically movable cyclindrical shaft, which made possible the contact between the Cu disc surface and the solution through a hanging meniscus arrangement with an appropriate meniscus height[22]. The potential of the working electrode was measured against a saturated $NaCl/Hg_2Cl_2/Hg$ electrode (*ssce*). A cylindrical Pt grid was used as counter-electrode. All measurements were made at 25.0 ± 0.1°C.

Solutions were prepared from twice-distilled water and a.r. chemicals, and purged with Ar. Electrochemical runs were made under Ar. Basically, the following aqueous solutions were employed: 0.002 M HaOH and 0.002 M NaOH + *y* M Na_2SO_4 ($2 \times 10^{-5} \leqslant y \leqslant 1$), so that the sulphate/hydroxide ion concentration ratio could be varied in the 0.01–500 range. Occasionally, variable amounts of dilute NaOH were added to *y*M Na_2SO_4 solutions to cover the $9 \leqslant pH \leqslant 11$ range. A conventional electrochemical circuitry was employed. Ohmic drop correction, even in dilute solutions, was insignificant.

A linear potential sweep in the $0.001\,V\,s^{-1} \leqslant v \leqslant 0.01\,V\,s^{-1}$ range was used to evaluate E_b, the critical breakdown potential. Average E_b values from five measurements at each v were obtained[23]. From the E_b vs. v plots, the value of E_b extrapolated to $v \Rightarrow 0$ was found.

Apparent current density (*j*) vs. potential (*E*) profiles resulting from both single (STPS) and repetitive triangular potential scans (RTPS) were run at $0.01\,V\,s^{-1}$ between cathodic (E_{sc}) and anodic (E_{sa}) switching potentials. Current transients were run by applying a constant potential step in the $-0.25 \leqslant E_s \leqslant 0.21$ V range. A new Cu specimen was used for each run.

Measurements of the Cu pitting induction time (t_i) were made with a new specimen in the following way. The specimen was cathodized in 0.002 M NaOH at −0.80 V for 4 min to produce a bare surface. Subsequently, a potential step to 0.90 V was applied, and the current transient was recorded at this potential. When the accumulated charge was about $4.0\,mC\,cm^{-2}$, a known amount of 0.002 M NaOH + 0.1 M Na_2SO_4 solution was added to the solution (about 5% total volume) to assure a minimum change in pH, and the potential was stepped to a value in the $0.20\,V \leqslant E_s \leqslant 0.55\,V$ range. Finally, the corresponding current transient was recorded. Reported values of t_i at each E_s correspond to the average value of 10 runs.

SEM micrographs were obtained with a Hitachi S-450 scanning electron microscope at beam energies in the 20–25 kV range.

3. RESULTS AND INTERPRETATION

3.1. *Current/potential profiles at low* v, *breakdown potentials*

The *j* vs. *E* profiles, recorded at $0.001\,V\,s^{-1}$ in 0.002 M NaOH + *y* M Na_2SO_4 ($10^{-2} \leqslant y \leqslant 1$) from −1.00 V upwards (Fig. 1), exhibit a cathodic current gradually decreasing to −0.30 V. As the potential becomes more positive than −0.30 V, an anodic current plateau which extends up to 0.20 V is observed. This current plateau has been assigned to the formation of a Cu oxide layer, and the simultaneous Cu electrodissolution through the Cu oxide layer[7]. However, at this low v value the oxide layer formation current is much smaller than that of the Cu electrodissolution. But as the applied potential exceeds *ca.* 0.20 V, a rapid anodic current increase is observed, and then a straight line in the *j* vs. *E* plot is approached. The transitions potential, resulting from the intercept of the straight line, corresponds to E_b, the critical breakdown potential of passivated Cu in the solution. Processes occurring at potentials more positive than E_b are mainly related to Cu pitting, as can be observed by SEM.

To attempt to correlate the critical sulphate/hydroxide concentration ratio for the appearance of pitting corrosion, the Cu behaviour was explored over a wide Na_2SO_4 concentration range. In the absence of sulphate ions in the solution, *ie* plain aqueous 0.002 M NaOH, the positive-going potential

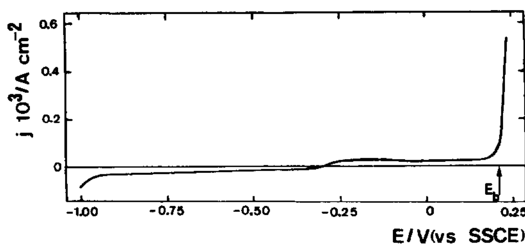

Fig. 1. Apparent current density (*j*) vs. potential (*E*) profiles of an annealed Cu specimen run at $v = 0.01\,V\,s^{-1}$ from $E_{s,c} = -1.00$ V upwards in 0.002 M NaOH + 0.01 M Na_2SO_4; 25°C. The arrow indicates the critical breakdown potential (E_b).

scan exhibits a passive region up 0.75 V, where the O_2 evolution reaction (OER) commences, whereas the reverse scan shows a small hysteresis loop which disappears at the same potential, for which $j \cong j_d$, the corrosion current of passivated Cu (Fig. 2a).

Otherwise, the addition of small amounts of Na_2SO_4 ($y < 10^{-4}$) does not significantly change the shape of the positive-going potential scan, in contrast to the reverse scan, which shows a remarkable hysteresis loop (Fig. 2b, c). In fact, the addition of Na_2SO_4 to 0.002 N NaOH promotes a localized Cu attack in the potential region where the OER takes place. This is accomplished by an increase in the Cu electrode area. Repassivation of pits formed in the OER potential range takes place at $E_r \cong 0$ V.

On the other hand, for $y \cong 10^{-4}$ M, current fluctuations related to the birth and death of pits initiate in the positive-going potential scan when the applied potential enters the OER range. These current fluctuations continue in the negative-going potential scan down to $E_r = 0.0$ V (Fig. 2c). For $y > 2.5 \times 10^{-4}$, the enhancement of pit birth and death in a rather broad potential range starting from 0 V upwards can be observed (Fig. 2d), although stable pitting can be formed in the OER potential range. This fact makes the evaluation of E_b rather uncertain. Finally, for $y > 10^{-3}$ M (Fig. 2e), the j vs. E profile reveals a well-defined E_b value for $E < E_{O_2}$, the OER threshold potential.

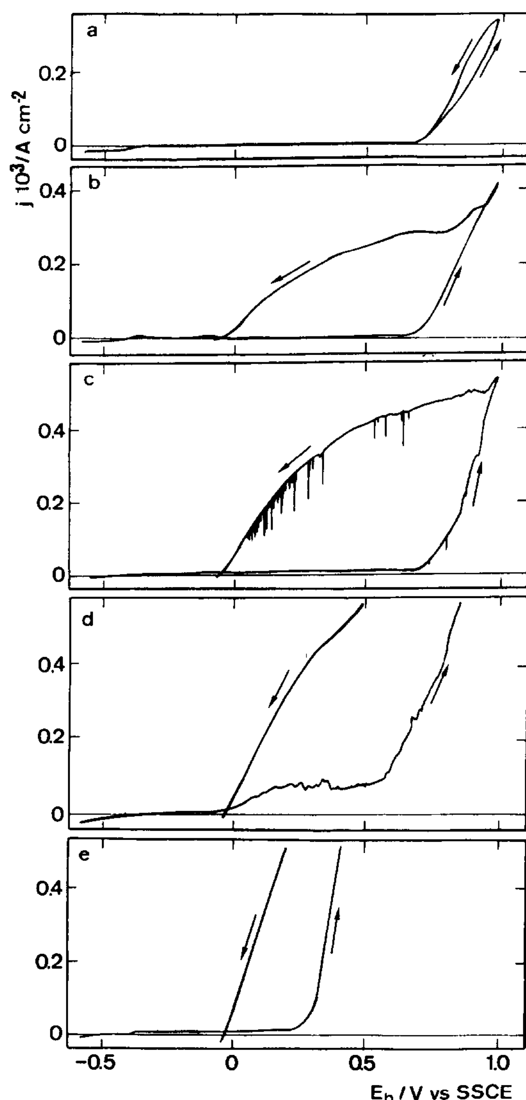

Fig. 2. Apparent current density (j) vs. potential (E) profile of annealed Cu specimens run at $v = 0.01$ V s^{-1} from $E_{s,c} = -1.00$ V upwards in 0.002 M NaOH + y M Na_2SO_4, for the following y values: (a) 0; (b) 2.4×10^{-5}; (c) 1.2×10^{-4}; (d) 5.1×10^{-4}; and (e) 1.2×10^{-3}; 25°C. Arrows indicate the potential scan direction.

The described results above indicate that there are three different regions in the E vs. log c plot (Fig. 3) after the addition of Na_2SO_4 to 0.002 M NaOH, where c is the Na_2SO_4 molarity in the solution. Thus, for $y < 2.5 \times 10^{-4}$ M, the critical breakdown potentials of Cu lie in the OER potential range, whereas in the $2.5 \times 10^{-4} < y < 10^{-3}$ range, unstable pitting can be observed at $E < E_{O_2}$. Only for $y > 10^{-3}$ M can a reliable value of E_b be determined. In this case, an increase in y shifts E_b negatively, according to a linear E_b vs. log c plot with a slope close of 0.085 V decade^{-1}. Further, the pH dependence on E_b can also be derived from the j vs. E plots at constant y and varying pH. Accordingly, a linear E_b vs. pH relationship is obtained with the slope $\Delta E_b/\Delta pH = -0.018$ V/pH unit. On the other hand, pit repassivation occurs at $E_r \cong 0.0$ V, irrespective of c.

3.2. *Voltammetry data*

Cyclovoltammograms were particularly aimed at determining the potential ranges of the different electrochemical reactions, and at selecting the most adequate operating conditions for potentiostatic experiments related to both the Cu oxide layer formation and Cu pitting.

For 1 M Na_2SO_4 + 0.002 M NaOH the first cyclovoltammogram run from $E_{s,c} = -1.20$ V to $E_{s,a} = 0.20$ V at $v = 0.01$ V s^{-1} (Fig. 4) shows region I extending from -0.30 V to *ca.* 0.06 V, which is related to Cu oxide layer formation, and region II covering from $E \simeq 0.06$ V upwards, which is associated with Cu pitting. The transition from region I to

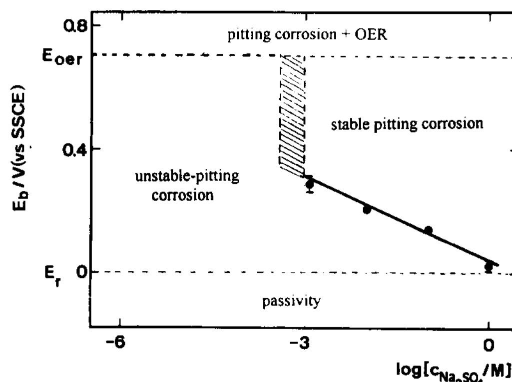

Fig. 3. Semilogarithmic plot of breakdown potential vs. Na_2SO_4 concentration; 25°C. Data correspond to j vs. E profiles run at $v = 0.01$ V s^{-1}. Definition of E_b in the dashed area is uncertain.

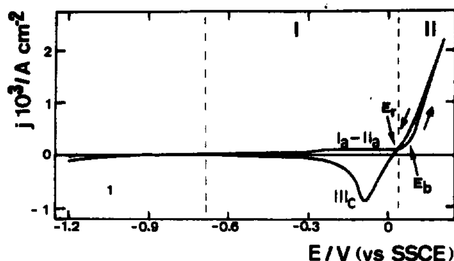

Fig. 4. Voltammogram of an annealed Cu specimen at $0.01\,V\,s^{-1}$; 0.002 M NaOH + 1 M Na_2SO_4; 25°C. Arrows indicate potential sweep directions and repassivation potential (E_r), and E_b values. I and II identify the Cu oxide layer and Cu electrodissolution region, and the Cu pitting corrosion region, respectively.

region II takes place at E_b. The nearly constant anodic current observed in region I can be considered as the sum of the Cu_2O and the CuO formation, together with the current of Cu electrodissolution through the passive layer[7]. Region II involves Cu pitting as the main process yielding soluble Cu^{2+} species, presumably as $HCuO_2^-$ anions at pH $\simeq$ 11. Macroscopic observation of specimens removed from the solution in region II shows both generalized attack and pitting. The subsequent reverse potential scan runs from 0.20 V downwards, exhibiting the typical hysteresis loop of pitting corrosion. The repassivating potential (E_r) is found at *ca.* 0.0 V, a value close to the potential where the anodic–cathodic current switching is observed. In addition, there is a broad and asymmetric cathodic peak (III_c) at -0.09 V, which corresponds to the electrodeposition of soluble Cu(II) species produced in region II. It should be noted that the above-described voltammetric behaviour is somewhat similar to that reported earlier for Cu in $NaClO_4$-containing media at the sample pH[15].

Stabilized cyclovoltammograms, *ie* those voltammograms which remain independent of the number of potential scans, run from $E_{s,c} = -1.20$ V to $E_{s,a} = 0$ V ($E_{sa} < E_b$) (Fig. 5) allowing us to establish the minimum number of reactions involved in Cu oxide layer formation. The positive-going potential scan starts to show an anodic current from -1.10 V upwards, which leads to a current plateau extending up to -0.40 V. It includes a broad, although very weak, peak with a point of inflexion at about -0.60 V, presumably related to the formation of the $Cu(OH)_{ad}$ submonolayer[7]. At potentials greater than -0.30 V, two anodic current peaks (I_a and II_a) are recorded, but peak II_a is not observed for $E_{s,a} < -0.15$ V. Peak I_a at -0.20 V and peak II_a at -0.12 V are related to Cu_2O and CuO–$Cu(OH)_2$ electroformation, respectively. When $E_{sa} < -0.30$ V, neither anodic nor cathodic current peaks are seen. In this case, only an anodic current contribution appears, even in the reverse scan down to -0.90 V. Under these conditions, the Cu oxide layer continues growing without further qualitative modifications. Otherwise, the reverse scan exhibits either peak I_c or peaks I_c and II_c, depending on whether $E_{sa} = -0.17$ V or $E_{sa} = -0.09$ V (Fig. 5). Peak II_c at -0.29 V and peak I_c at -0.45 V are assigned to the electroreduction of CuO–$Cu(OH)_2$ to Cu_2O, and to the electroreduction of Cu_2O to Cu, respectively[10]. Finally, a small peak IV_c appears at -1.10 V, just at the beginning of the hydrogen evolution reaction (HER). The HER contribution extends from -0.90 V downwards. The value of q_a/q_c, the anodic to cathodic voltammetric charge density ratio, varies with E_{sa}, as given in Table 1. In the $-0.30 \leqslant E_{sa} \leqslant 0$ V range, that ratio decreases with $E_{s,a}$. These results are consistent with the formation of soluble Cu(I) species already observed at potentials lower than -0.30 V[7, 8]. For $E_{s,a} > -0.30$ V, the formation of the Cu oxide film hinders the electrodissolution of Cu as soluble Cu(I) or Cu(II) species in the solution. However, as the value

Table 1. Values of the anodic to cathodic charge ratio determined from the stabilized voltammograms recorded for different $E_{s,a}$ (Fig. 5)

E_{sa} (V)	$q_a \times 10^3$ (C cm^{-2})	$q_c \times 10^3$ (C cm^{-2})	q_a/q_c
-0.30	0.288	0	$\Rightarrow \infty$
-0.17	0.571	0.203	2.81
-0.09	0.824	0.397	2.08
0	1.102	0.579	1.90
0.20	195.1	62.72	3.11

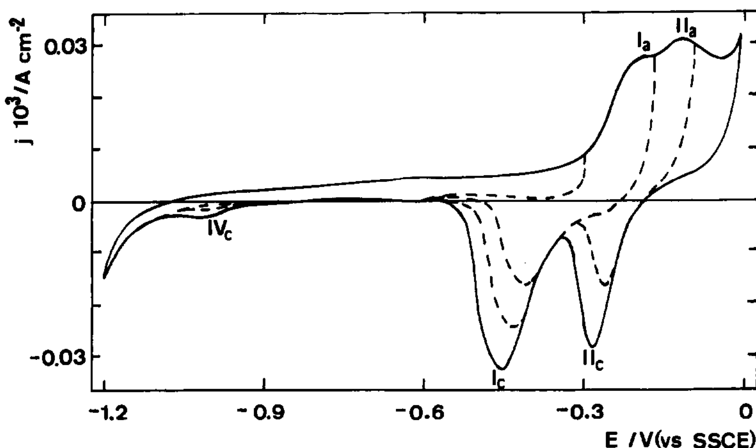

Fig. 5. Stabilized voltammogram of an annealed Cu specimen run at $0.01\,V\,s^{-1}$ changing $E_{s,a}$; 0.002 M NaOH + 1 M Na_2SO_4; 25°C.

of E_b is approached, an increase in the q_a/q_c ratio is observed.

Generally, the above cyclovoltammetric features depend on pH and Na_2SO_4 concentration (Fig. 6). The value of E_b shifts negatively as the pH is decreased at constant y. Consequently, both peaks II_a and II_c are no longer observed at pH 9. Furthermore, an increase in pH results in a negative potential shift of peaks I_a, I_c and IV_c. The comparison between Fig. 6b and c allows us to conclude that, at a constant pH, the influence of Na_2SO_4 concentration on the voltammetric features reflects principally on the value of E_b (Fig. 3), and on the relative height of those peaks located in the -0.8 to -1.2 V range.

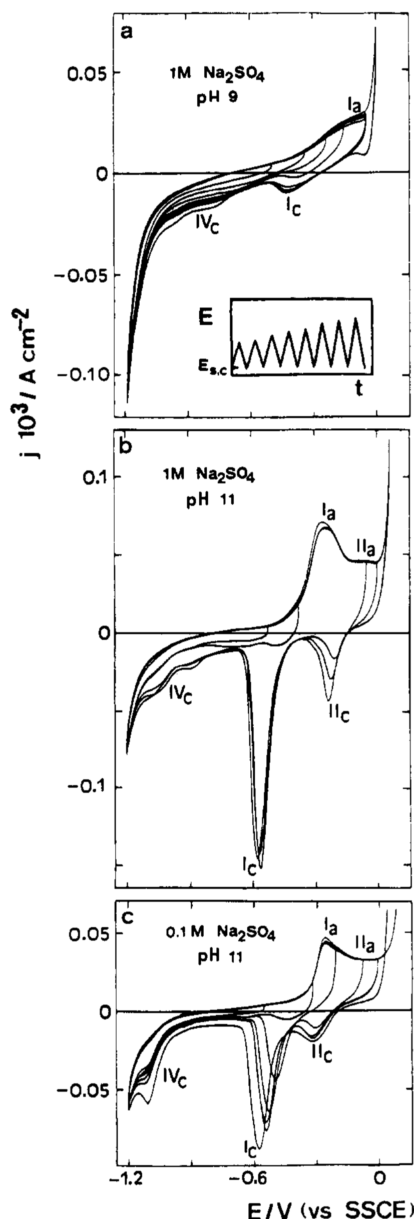

Fig. 6. Stabilized voltammograms of annealed Cu specimens at 0.01 V s^{-1} for different pH and Na_2SO_4 concentrations; 25°C. The potential routine is shown in the inset.

3.3. *Potentiostatic current transients*

Potentiostatic current transients were run for both $E_s < E_b$ and $E_s > E_b$, after applying a specific two potential step electrode pretreatment. A new Cu specimen was used for each run.

For $E_s < E_b$, the electrode was first held at $E_c = -1.20$ V for 4 min to assure an electroreduced Cu surface, then the potential was stepped to -0.40 V for 100 s to produce a fixed amount of Cu oxide coating, and immediately afterwards the potential was set to E_s for current transient recording. The potentiostatic current transients run in 0.002 M NaOH + 1 M Na_2SO_4 for $-0.25\ \text{V} < E_s < 0$ V show a continuous anodic current decrease until the quasi-steady Cu electrodissolution current through the Cu oxide layer has been attained (Fig. 7).

Otherwise, for $E_s > E_b$, Cu specimens were previously held at -1.20 V for 4 min, subsequently potential-stepped to -0.025 V for 100 s to form a stationary Cu oxide coating, and finally, potential-stepped to $0.15 \leqslant E_s \leqslant 0.24$ V to obtain the anodic current transient. In these transients (Fig. 8) the current initially decreases to I_m, the minimum current reading at time t_i, and then increases to approach a steady value. The value of t_i which can be considered as an induction time for Cu pitting decreases as E_s is positively shifted. In order to obtain more accurate values of t_i, current transients and $E_s > E_b$ were recorded in 0.01 M Na_2SO_4 + 0.002 M NaOH. As in this solution, longer and more accurate t_i values than in 1 M Na_2SO_4 + 0.002 M NaOH were determined. Data show that t_i decreases markedly on increasing the $(E_s - E_b)$ difference (Fig. 9).

3.4. *SEM micrographs*

SEM micrographs of annealed and electropolished (blanks) Cu specimens reveal rather large, rounded Cu grains (Fig. 10a), and small hemispherical randomly distributed micropits. Micrographs of Cu specimens subjected to anodization in region I (Fig.

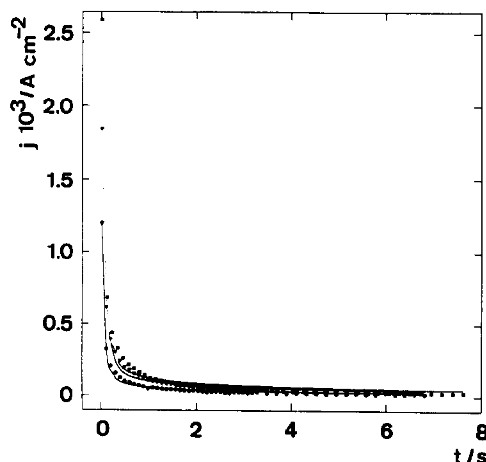

Fig. 7. Current transients obtained at $E_s < E_b$; 0.002 M NaOH + 1 M Na_2SO_4; 25°C. Symbols denote experimental data and solid lines correspond to current transients calculated with equations (11) and (12). E_s values: (●) -0.20 V; (▼) -0.10 V; and (■) 0 V.

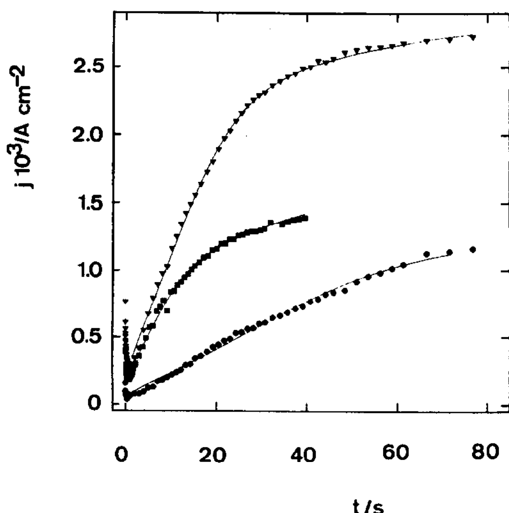

Fig. 8. Current transients recorded at $E_s > E_b$; 0.002 M NaOH + 1 M Na_2SO_4; 25°C. Symbols denote experimental data and solid lines currespond to current transients calculated from equations (11), (16) and (17). E_s values: (●) 0.175 V; (■) 0.21 V; and (▼) 0.24 V.

10b) resemble the blank, although the details are rather veiled by a thin coating.

On the other hand, the micrograph of Cu specimens anodized in region II (Fig. 10c) show crystallographic pits together with corrosion products located around the pits. At the highest positive potentials, corrosion products inside large pits can also be seen (Fig. 10d). Both pit density and average pit size increase as E_s is shifted positively.

4. DISCUSSION

4.1. *Preliminary considerations*

Several complex electrochemical processes are involved in the anodization of Cu in alkaline Na_2SO_4-containing alkaline solutions[20]. The initial reaction leading to the electroformation of a Cu oxide film at pH ≅ 11 is accompanied by the appearance of soluble species, such as $Cu_2O_2H^-$

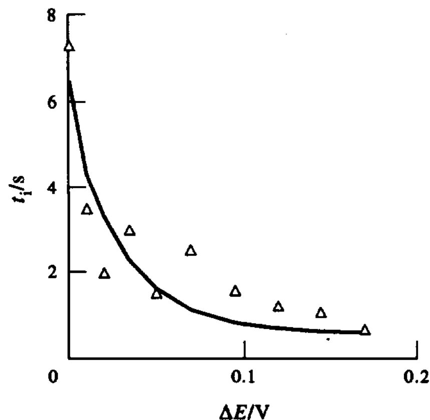

Fig. 9. t_i vs. $(E_s - E_b)$ plot; (Δ) experimental data, (——) calculated with equation (8).

produced either from $Cu(OH)_{ad}$ or Cu_2O[4, 8, 24, 25]. The formation of soluble Cu(I) species can explain the complex voltammetric response resulting in the −1.00 to −0.50 V range[25]. Otherwise, in the absence of Na_2SO_4, the largest amount of soluble Cu(I) species is formed for $E_{s,a} < -0.30$ V[7].

From the voltammograms run at different E_{sa} (Fig. 5), it appears that the anodic layer is predominantly composed either of Cu_2O or a mixture of Cu_2O and CuO or $Cu(OH)_2$, depending on whether $E_{s,a} \simeq -0.20$ V or $E_{s,a} \simeq -0.10$ V, as peaks II_c and I_c are located in the potential range predicted by thermodynamics for the following electroreduction reactions:

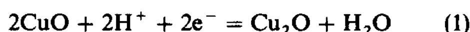

$$2CuO + 2H^+ + 2e^- = Cu_2O + H_2O \qquad (1)$$

and

$$Cu_2O + 2H^+ + 2e^- = 2Cu + H_2O, \qquad (2)$$

where the reversible potentials of reactions (1) and (2) are $E_{rev}(1) = -0.23$ V and $E_{rev}(2) = -0.43$ V at pH 11 and 25°C, respectively[26]. Under these circumstances, the formation of both Cu oxides and soluble Cu species has been observed[7, 8].

On the other hand, when $E_{sa} > 0$ V, both the rupture of the oxide film and Cu pitting are assisted by the presence of Na_2SO_4 in the solution. In this case, the main corrosion product is either $HCuO_2^-$ or Cu^{2+}. The formation of Cu^{2+} species would be favoured by the local decrease in pH at the pit surface. According to thermodynamics[26], the electroreduction of $HCuO_2^-$ to Cu_2O or Cu can be assigned to the following overall reactions:

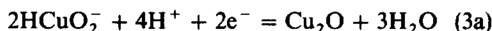

$$2HCuO_2^- + 4H^+ + 2e^- = Cu_2O + 3H_2O \qquad (3a)$$

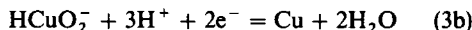

$$HCuO_2^- + 3H^+ + 2e^- = Cu + 2H_2O \qquad (3b)$$

and $E_{rev}(3a) = 0.365 + 0.0591 \log(HCuO_2^-) + 0.1182 \log(H^+)$, and $E_{rev}(3b) = 0.005 + 0.0295 \log(HCuO_2^-) + 0.0886 \log(H^+)$, at 25°C, respectively. Reaction (3b) is related to the complex peak III_c (Fig. 4).

Therefore, the comparison between voltammograms run in Na_2SO_4-containing solution and those resulting in plain NaOH under equivalent conditions[27] reveals the considerable influence of Na_2SO_4 on the electrochemical behaviour of Cu in alkaline solutions, particularly by assisting electrooxidation processes. In fact, the anodic voltammetric charge resulting in the potential range in which Cu oxide formation and Cu electrodissolution are the main processes through the oxide coating (Fig. 5) is always greater than the complementary cathodic charge, independently of $E_{s,a}$. This fact is consistent with the previous observation that, for constant ionic strength in Na_2SO_4-containing solutions, the slope of the Cu_2O electroformation current peak vs. square root of the speed of the rotating Cu disk electrode is greater than that of plain NaOH. These results suggest that the competitive adsorption between OH^- and sulphate ions should play an important role already at the early stages of Cu oxide layer formation, through a number of equilibrium reactions, such as

$$Cu + OH^- = Cu(OH^-) \qquad (4)$$

Fig. 10. SEM micrographs of electropolished Cu specimens obtained at different magnifications, (a) before (blank), (b–d) after 100 s anodization in 0.002 M NaOH + 1 M Na_2SO_4 : (b) $E_s = 0$ V; (c) $E_s =$ 0.18 V; and (d) $E_s = 0.25$ V; 25°C.

$$Cu(OH^-) + SO_4^{2-} = Cu(SO_4^{2-}) + OH^- \quad (5)$$

or

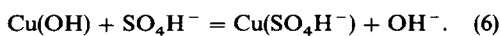

$$Cu(OH) + SO_4H^- = Cu(SO_4H^-) + OH^-. \quad (6)$$

In these reactions, parentheses denote adsorbed species which act as precursors for Cu electro-oxidation via Cu_2O, $Cu(OH)_2$ and soluble Cu species. These reactions can explain the increase in the Cu electrodissolution current in Na_2SO_4 solutions. In fact, competitive adsorption reactions should be considered in the reaction pathway already proposed for Cu electro-oxidation in base solutions[8], in order to extend the validity of the proposed reaction mechanism to other aqueous electrolytic environments.

4.2. *Pit initiation on* Cu *in* Na_2SO_4*-containing alkaline solutions*

The presence of Na_2SO_4 also produces passivity breakdown of Cu in alkaline solutions. The effect for

sulphate anions on this process is clearly revealed by the decrease in the value of E_b with the increase in the Na_2SO_4 concentration. This is an indication of the strong interactions between the passivated Cu surface and sulphate ions, which become even stronger as the applied potential is shifted positively. Runs performed at different pH and Na_2SO_4 concentration allowed us to admit that if there is a critical OH^-/SO_4^{2-} molar concentration ratio for Cu pitting in these solutions, its value should be greater than 10^2). It appears that the nature of the Cu oxide passivating layer depends considerably on this ratio. Thus, when it is greater than 10^2, the aggressive behaviour of sulphate ions is hindered by OH^- ions, favouring the formation of a stable Cu oxide layer. But as it is further decreased, sulphate ions make the passive layer more prone to attack. Accordingly, the behaviour of the system approaches that recently described for the breakdown of passive films on Cu in HCO_3^- solutions containing SO_4^{2-} ions[21].

The above interpretation explains the dependence of E_b on Na_2SO_4 concentration at a constant pH, as given by the equation

$$E_b = C + b \log c_{Na_2SO_4}, \quad (7)$$

where C is the breakdown potential for $c_{Na_2SO_4} =$ 1 M.

According to the point defect model[29], passivity breakdown is due to the diffusion of vacancies from the metal/oxide interface to the oxide/solution interface, enhanced by anion adsorption. In this model $b = 2.3RT/\alpha F$, where α represents the dependence of the electric field drop across the film/solution interface on the applied potential. Thus, by using $b = 0.08\ \mathrm{V\ dec^{-1}}$, $\alpha \cong 0.75$.

On the other hand, from the point defect model, the potential dependence of t_i is given by the equation

$$t_i = \xi' \, e^{xF\alpha(E_s - E_b)/2RT} + \tau, \quad (8)$$

where τ is the time required for vacancy diffusion, x is the cation charge, and ξ' is

$$\xi' = \xi/j_0 \, \mu^{-x/2}(a_{Cl}-)^{x/2} e^{xF\alpha E_b/zRT}, \quad (8a)$$

ξ being the critical amount of accumulated metal holes, and the expression for j_0 is given by

$$j_0 = xKD(N/\Omega)^{1+X/2} e^{\Delta G^0/RT}, \quad (8b)$$

where Ω is the molecular volume per cation, D is the diffusivity of metal vacancies, N is Avogadro's number, K is a constant, μ is the chemical potential, and ΔG^0 is the free energy for the Schottky pair reaction. The present results can be fitted with $\xi = 6$, $\tau = 0.50$ s, $x = 2$ and $\alpha = 0.8$ (Fig. 9), leading to a reasonable agreement between α values estimated from equations (7) and (8). It should be noted, however, that in Na_2SO_4-containing alkaline solutions the value of α is greater than that recently reported for aqueous solutions containing carbonate and sulphate anions[21]. Attempts to fit experimental results with other passivity breakdown models[21] led to poorer results. Therefore, as it has been recently suggested[21], the point defect model offers, at present, the best explanation for the initial stage of Cu pitting in Na_2SO_4-containing alkaline solutions.

4.3. *Pit growth kinetics of* Cu *in* Na_2SO_4*-containing alkaline solutions*

Following pit nucleation, the localized corrosion of Cu actually implies a pit growth process[30] at a defective passive metal surface. Current transients associated with pit growth involve different contributions, which can be independently evaluated by adequately selecting both the potential and time windows. To discriminate the different current contributions, it is convenient to analyse first those current transients recorded at $E_s < E_b$.

Thus, for $E_s < E_b$, the overall anodic current density (j_t), can be interpreted as a sum of several terms, namely, the apparent current density associated with the double-layer charging (j_{dl}), a term related to the Cu oxide layer formation (j_p), and a term related to Cu electrodissolution through the Cu oxide coating (j_d). Thus[30],

$$j_t = j_{dl} + j_p + j_d. \quad (9)$$

The double-layer charging component drops to zero in time, therefore, in the time domain of this study, its contribution can be neglected. Accordingly, equation (9) reduces to

$$j_t = j_p + j_d. \quad (10)$$

The term j_p in equation (10) is specifically related to the growth of the Cu oxide coating which can be described as an instantaneous nucleation and circular two-dimensional growth under diffusion control. The corresponding rate equation is[31]

$$j_p = P_1 \exp(-P_2 t), \quad (11)$$

where

$$P_1 = K'\pi q D N_0 \quad (11a)$$

$$P_2 = K'\pi D N_0 \quad (11b)$$

$$P_1/P_2 = q, \quad (11c)$$

q is the apparent charge density involved in the formation of the Cu oxide layer, D is the diffusion coefficient of species involved in the oxide layer growth, N_0 is the number of sites available for nucleation, the K' is a proportionality constant.

The term j_d in equation (10) represents the rate of Cu electrodissolution through the oxide coating, which can be interpreted as a linear diffusion controlled process[32] expressed by the equation

$$j_d = P_3 t^{-1/2}, \quad (12)$$

where

$$P_3 = zF\pi^{-1/2} D_i^{1/2} \Delta c \quad (12a)$$

and D_i and Δc are the diffusion coefficients and the concentration gradient of the diffusion species through the Cu/Cu oxide coating, respectively.

By using equations (10)–(12), current transitions recorded at $E_s < E_b$ (Fig. 7) can be reproduced with the set of parameters assembled in Table 2.

Table 2. Parameters used for curve fitting with equations (11) and (12), as shown in Fig. 7

E_s (V)	P_1 (mA cm^{-2})	P_2 (s^{-1})	P_3 (mA s$^{1/2}$ cm^{-2})	q (mC cm^{-2})
−0.25	0.30	21	0.04	0.014
−0.20	0.93	15	0.06	0.062
−0.15	1.9	17	0.09	0.11
−0.10	1.2	10	0.10	0.16
−0.05	2.0	12	0.12	0.16
0	1.6	13	0.17	0.12

Considering the duplex passive layer structure of Cu oxide coatings electrochemically formed, the value of q, resulting from the P_1/P_2 ratio at each E_s, can be assigned to the inner part of the oxide layer, which consists principally of Cu_2O. Values of q increase from 0.014 mC cm^{-2} at $E_s = -0.25$ V, a potential at which the surface coverage is below the expected saturation coverage, *ie* 0.210 mC cm^{-2} for Cu_2O[7], to a maximum coverage attained in the −0.10 to −0.05 V range. At these potentials, about 80% of the total surface is covered by Cu_2O species. At the maximum coverage, the average thickness (h) of the Cu_2O layer can be estimated from the equation

$$h = MP_1/zF\rho P_2, \quad (13)$$

taking $M = 143$ g mol^{-1}, $\rho = 6.0$ g cm^{-3}, and $z = 1$. Then, from equation (13), $h \simeq 0.4$ nm, a figure which is consistent with the thickness expected from a hydrous Cu_2O monolayer. As $E_s \Rightarrow E_b$, a decrease in the value of q can be noted.

Otherwise, the value of P_2 is almost independent of E_s, a fact which indicates that in region I (Fig. 4) the number of nucleation sites remains practically constant in agreement with the predictions of the model. Conversely, the value of P_3 increases with E_s to reach a nearly constant value when $E_s \geqslant -0.10$ V. The P_3 potential dependence should be attributed to a potential-dependent Δc value, which also reaches a limiting value at high positive potentials. As the potential is increased, a maximum potential-independent, concentration gradient of the reacting species should be reached. Under these conditions, Δc can be related to c*, the maximum concentration of the reacting species at the Cu/Cu oxide layer interface (Cu^{2+}). Accordingly, provided that $\Delta c^* \cong 6 \times 10^{-2}$ mol cm^{-3}[7], the maximum value of D is *ca.* 10^{-15} cm^2 s^{-1}, a figure which is consistent with Cu electrodissolution involving the diffusion of Cu^{2+} ions across the Cu oxide layer.

Let us consider now those current transients resulting from $E_b > E_s$. In this case, two new current contributions to j_t must be considered, i.e. one term (j_c) related to the Cu pitting, and another term ($J_{d'}$) associated with a non-uniform Cu corrosion through a basic sulphate layer. Then,

$$j_t = j_p + j_d + j_{d'} + j_c, \quad (14)$$

where $j_{d'}$ involves the Cu electrodissolution of Cu through the passive layer influenced by the presence of sulphate ions. At this stage, it is reasonable to admit that the condition $j_d \ll j_{d'}$ is applicable to the results shown in Fig. 8. Then,

$$j_t = j_p + j_c + j_{d'}. \quad (15)$$

The term $j_{p'}$ in equation (15) is given by equation (11), and new expressions should be considered for $j_{d'}$ and j_c.

The term $j_{d'}$ represents Cu electrodissolution through a basic Cu salt layer formed at certain regions of the electrode surface. Under these circumstances, Cu electrodissolution can be described as a three-dimensional nucleation and hemispherical growth under diffusion control. Correspondingly, the expression for $j_{d'}$ is[32]

$$j_{d'} = P_6 t^{-1/2}[1 - \exp(-P_7 t)], \quad (16)$$

with

$$P_6 = zF\pi^{-1/2}D'^{1/2}\,\Delta c' \quad (16a)$$

$$P_7 = K'\pi D' N_{os} \quad (16b)$$

$$K = (8\pi M\,\Delta c')^{1/2}\rho^{-1/2}, \quad (16c)$$

where D' is the diffusion coefficient of Cu ions in the solution, N_{os} stands for the number of sites for pit growth, and $\Delta c'$ is the concentration gradient of Cu(II) ionic species at the salt/solution interface which in turn, is determined by the solubility of Cu salts in the solution.

The corrosion of Cu at pits can be tentatively explained in terms of an instantaneous nucleation and three-dimensonal conical pit growth charge transfer control. The kinetic equation for such a process is of the following form[33]:

$$j_c = P_4[1 - \exp(-P_5 t^2)], \quad (17)$$

with

$$P_4 = zFk \quad (17a)$$

$$P_5 = \pi M^2 N_0 k'^2 \rho^{-2}, \quad (17b)$$

N_0 is the number of sites available for pit nucleation, M and ρ are the atomic weight and the density of Cu, respectively, and k and k' are the apparent rate

Table 3. Parameters used for curve fitting with equations (11), (16) and (17), as shown in Fig. 8

E_s (V)	P_1 (mA cm^{-2})	P_2 (s^{-1})	P_4 (mA cm^{-2})	P_5 (s^{-2})	P_6 (mA s$^{1/2}$ cm^{-2})	P_7 (s^{-1})
0.140	0.12	123	0.64	0.02	63	0.02
0.175	0.34	137	0.62	0.37	28	0.20
0.210	0.44	95	0.36	0.20	27	0.14
0.240	0.65	60	1.11	0.05	28	0.15

constants for pit growth in the directions perpendicular and parallel to the corroding surface plane. respectively. By using equations (11), (16) and (17), current transients shown in Fig. 8 can be reproduced with the set of parameters assembled in Table 3.

Values of P_1 and P_2 are comparable to those shown in Table 2, at least within one order of magnitude. It should be noted, however, that the increase of P_2 in region II (Fig. 4) can be assigned to an increase in active area, *ie* seemingly, a roughness factor of about five appears in the E_s range covered by experiments. Otherwise, the decrease in the value of P_2 by a factor of two would indicate that N_0 decrease with E_s because the actual portion of the Cu surface available for oxide layer formation is diminished. Furthermore, from the P_1/P_2 ratio, it can be concluded that the contribution to Cu_2O oxide formation is drastically reduced in region II (Fig. 4). The values of P_6 and P_7 remain appreciably constant, at least within the errors of this work, in agreement with the expectation of a diffusion controlled process. In contrast the fluctuations in the values of P_4 and P_5 impede an adequate evaluation of their potential dependences as would be expected from a charge transfer controlled reaction.

5. CONCLUSIONS

The electrochemical behaviour of Cu in alkaline solutions depends considerably on the Na_2SO_4 concentration. The presence of this salt produces an enhancement of Cu electrodissolution through the passive layer, and decreases the passivity breakdown potential.

There is a critical OH^-/sulphate concentration ratio for the onset of localized corrosion in these solutions. A very early competitive interaction between OH^- and sulphate ions at the passive layer may play an important role in the kinetics of the overall process.

Pit initiation can, in principle, be explained by the point defect model for passivity breakdown.

Pit nucleation and growth involve a number of contributions which can be distinguished through the analysis of current transients at constant potential by using nucleation and growth models.

Acknowledgements—Financial support for this work by UNELCO S.A. (Unión Eléctrica de Canarias S.A.) and by the Gobierno de Canarias (Dirección General de Universidades e Investigación) under contract no. 91/18, is gratefully acknowledged.

REFERENCES

1. D. W. Shoesmith, T. E. Rummery, D. Owen and W. Lee, *J. electrochem. Soc.* **123,** 790 (1976).
2. V. Ashworth and D. Fairhust, *J. electrochem. Soc.* **124,** 506 (1977).
3. J. van Muylder, in *Comprehensive Treatise of Electrochemistry* (Edited by J. O'M. Bockris, B. E. Conway, E. Yeager and R. E. White), Vol. 4, pp. 1–96. Plenum Press, New York (1981).
4. M. R. G. de Chialvo, R. C. Salvarezza and A. J. Arvia, *J. appl. Electrochem.* **14,** 165 (1984).
5. H. H. Strehblow and H. D. Speckmann, *Werkstoffe Korros,* **35,** 512 (1984).
6. H. D. Speckmann, M. M. Lohrengel, J. W. Schultze and H. H. Strehblow, *Ber. Bunsenges. Phys. Chem.* **89,** 392 (1985).
7. M. R. G. de Chialvo, R. C. Salvarezza, D. Vásquez Moll and A. J. Arvia, *Electrochim. Acta* **30,** 1501 (1985).
8. M. R. G. de Chialvo, J. O. Zerbino, S. L. Marchiano and A. J. Arvia, *J. appl. Electrochem.* **16,** 517 (1986).
9. M. Wanner, H. Wiese and K. G. Weil, *Ber. Bunsenges. Phys. Chem.* **92,** 736 (1988).
10. J. Gómez Becerra, R. C. Salvarezza and A. J. Arvia, *Electrochim. Acta* **33,** 613 (1988).
11. M. Pérez Sánchez, M. Barrera, S. González, R. M. Souto, R. C. Salvarezza and A. J. Arvia, *Electrochim. Acta* **35,** 1337 (1990).
12. M. M. Laz, R. M. Souto, S. González, R. C. Salvarezza and A. J. Arvia, *Electrochim. Acta* **37,** 655 (1992).
13. M. G. Figueroa, R. C. Salvarezza and A. J. Arvia, *Electrochim. Acta* **31,** 655 (1986).
14. M. R. G. de Chialvo, M. F. L. de Mele, R. C. Salvarezza and A. J. Arvia, *Corros. Sci.* **28,** 121 (1988).
15. R. M. Souto, M. Pérez Sánchez, M. Barrera, S. González, R. C. Salvarezza and A. J. Arvia, *Electrochim. Acta* **38,** 703 (1993).
16. M. G. Figueroa, R. C. Salvarezza and A. J. Arvia, *Electrochim. Acta* **31,** 671 (1986).
17. M. G. Figueroa, M. F. L. de Mele, R. C. Salvarezza and A. J. Arvia, *Electrochim. Acta* **32,** 231 (1987).
18. D. Vásquez Moll, M. R. G. de Chialvo, R. C. Salvarezza and A. J. Arvia, *Electrochim. Acta* **30,** 1011 (1985).
19. T. Hurlen, G. Ottesen and A. Staurset, *Electrochim. Acta* **23,** 39 (1978).
20. I. T. E. Fonseca, A. C. S. Marin and A. C. Sá, *Electrochim. Acta* **37,** 2541 (1993).
21. I. Milošev, M. Metifkoš-Hubovic, M. Drogowska, H. Ménard and L. Brossard, *J. electrochem. Soc.* **139,** 2409 (1992).
22. D. Dickertmann, F. D. Koppitz and J. W. Schultze, *Electrochim. Acta* **21,** 967 (1976).
23. M. Janik-Czachor, *Werkstoffe Korros.* **31,** 606 (1980).
24. B. Miller, *J. electrochem. Soc.* **116,** 1675 (1969).
25. S. L. Marchiano, C. I. Elsner and A. J. Arvia, *J. appl. Electrochem.* **10,** 365 (1980).
26. M. Pourbaix, *Atlas of Electrochemical Equilibria in Aqueous Solutions.* Pergamon Press, Oxford (1966).
27. A. M. Castro Luna de Medina, S. L. Marchiano and A. J. Arvia, *J. appl. Electrochem.* **8,** 121 (1978).
28. D. V. Vasquez Mol. R. C. Salvarezza, H. Videla and A. J. Arvia, *J. electrochem. Soc.* **132,** 754 (1985).
29. L. F. Lin, C. Y. Chao and D. D. MacDonald, *J. electrochem. Soc.* **128,** 1194 (1981).
30. R. C. Salvarezza, D. V. Vásquez Moll and A. J. Arvia, *Electrochim. Acta* **32,** 1421 (1987).
31. W. Davison and J. A. Harrison, *J. electroanal. Chem.* **44,** 213 (1973).
32. B. Scharifker and G. Hills, *Electrochim. Acta* **28,** 879 (1983).
33. M. Y. Abyaneh and M. Fleischmann, *Electrochim. Acta* **27,** 1513 (1982).